

Visual Tracking and LIDAR Relative Positioning for Automated Launch and Recovery of an Unmanned Rotorcraft from Ships at Sea

■ MATT GARRATT, HEMANSHU POTA, ANDREW LAMBERT, SEBASTIEN ECKERSLEY-MASLIN, AND CLEMENT FARABET

Abstract

Sensors and systems for a fully autonomous unmanned helicopter have been developed with the aim of completely automating the landing and launch of a small-unmanned helicopter from the deck of a ship. For our scheme, we have combined a laser rangefinder (LRF) system with a visual tracking sensor to construct a low-cost guidance system. Our novel LRF system determines both the distance to and the orientation of the deck in one cycle. We have constructed an optical sensor to complement the laser system, comprising a digital camera interfaced to a Field Programmable Gate Array (FPGA), which enables the entire target tracking computation to be achieved in a very small self-contained form factor. A narrowband light source on the deck is detected by the digital camera and tracked by an algorithm implemented on the FPGA to provide a relative bearing to the deck from the helicopter. By combining the optical sensor bearing with the information from the laser system, an accurate estimate of the helicopter position relative to the deck can be found.

Introduction

Determining the relative position and orientation of a pitching and heaving deck is a major challenge. Previous attempts at doing this have predominantly focused on using either (a) a relative global positioning system (GPS), which is subject to satellite availability, signal blockage from the ship's superstructure, multipath errors, and jamming (Pervan et al. 2003; Gold and Brown 2004), or (b) radar guidance, which is expensive and reliant on substantial radio frequency emissions.

As part of the US Department of Defense Joint Precision Approach and Landing System project (USAF 1994), research is being funded on means to make Shipboard Relative GPS sufficiently robust in the presence of errors to permit automatic landings on aircraft carriers (Belton et al.

1999; Gold and Brown 2005). This work is progressing but it is likely that, for robust operations on small ships, the use of ship-based navigation beacons known as *pseudolites* may be required to augment satellite signals close to the ship (Montgomery et al. 1999). Two of the main ship launched VTOL UAVs that have been under development, Northrop Grumman Fire-scout and Bell Eagle Eye, make use of the UAV Common Automatic Recover System (UCARS) developed by Sierra Nevada Corp (2008). The UCARS uses a millimeter-wave radar on the ship in combination with a transponder mounted on the aircraft to track the trajectory of the UAV. While the UCARS is effective, it requires the use of radar emissions, which can be undesirable in a tactical situation. In addition, we are constrained to using lighter weight systems onboard the UAV owing to the much-reduced payload

capability of a small VTOL UAV (30 kg for the R-Max).

In our approach, we have assumed that the UAV can complete its mission, including waypointing, using a mature navigation technology such as GPS. Submeter accuracy relative to a moving base (i.e., the ship) is achievable with current COTS solutions such as the NovAtel moving base option (NovAtel 2004; Ford et al. 2005), which would require a single GPS receiver on the ship and another on the UAV with a low bandwidth data link between them. We assume that this technology is sufficient to get the UAV to a keypoint over the deck of the ship. For the final descent and landing phase, we propose a new precision guidance system that incorporates an accurate estimate of the ship motion and a sensor for measuring the instantaneous orientation and location of the landing deck. We are also developing a simple yet robust algorithm for predicting ship motion that will be used in conjunction with the new sensors to assist in trajectory planning, with the ultimate aim of landing the UAV on the deck at an instant where the deck motion is at a minima.

As the primary sensor, we have modified an existing laser rangefinder (LRF) device with a novel scanning mechanism that determines both the distance to and the orientation of the deck in one cycle. We have constructed a downward-looking optical sensor to complement the laser system. The sensor comprises a digital camera interfaced to a Field Programmable Gate Array (FPGA) on a single printed circuit board. A narrowband light source on the deck is detected by the digital camera and tracked by an algorithm implemented on the FPGA to provide a relative bearing to the deck from the helicopter. By combining the optical sensor bearing with the information from the laser system, the exact position of the helicopter relative to the deck can be found. In this paper, we discuss the algorithms used and present some flight test results for our deck attitude sensing system (DASS).

To test the algorithms, we have also constructed a three-degrees-of-freedom moving deck plat-

form to simulate the motion of a seagoing vessel. The deck is capable of pitch and roll up to 25° and heave up to 1 m and will be used to dynamically test the landing systems.

System Overview

Experiments for this research were conducted on the 80 kg Yamaha R-Max helicopter shown in **Figure 1**. This platform has been used for autonomous helicopter research at a number of other institutions including Georgia Tech (Johnson and Schrage 2003), UC Berkeley (Kim et al. 2002), Linköping University (Doherty 2004), Carnegie Mellon University (Charles 1998), and NASA/US Army (Whalley et al. 2003). The Yamaha R-Max platform is predominantly used for agricultural work in Japan, although a fully autonomous version has been marketed for airborne surveillance. A number of variants have been produced but the underlying systems are similar in each model. Our vehicle is an L-15 R-Max with a 30 kg payload and an endurance of approximately 1 hour. The performance of the R-Max makes it an ideal platform for research. The R-Max comes with a stability augmentation system based on an attitude control inner loop. The Yamaha control system is known as the Yamaha Attitude Control System (YACS). The YACS on our R-Max has been configured to output inertial information to our system via an RS-232 link that includes the output of three fiber optic rate gyroscopes and three accelerometers. We have added a *Microstrain 3DM-GX1* attitude sensor, which incorporates a three-axis magnetometer, to the R-Max to provide heading information into the flight computer.

Our avionics system includes a processing unit comprising a PC104 computer that is interfaced to the LRF, a radio modem, a Novatel RT2 RTK DGPS, and the YACS. Currently, our PC104 computer runs the RTLinuxPro real-time operating system and flight control software that performs sensor fusion and generates the control inputs to drive the collective, cyclic, and tail rotor servos. The PC104 software includes an algorithm to find the plane of the deck from the laser data.

DASS

Our DASS comprises a LRF with a spinning mirror as shown in **Figure 2**. Owing to the orientation of the axis of the mirror and the angle of the mirror to the axis, the laser scans a conical pattern centered on the deck below. As the laser traces out an oval of points on the deck, an array of three-dimensional (3D) coordinates is assembled that defines the intersection of the laser scan pattern and the deck. Each scan takes place in less than 40 ms and typically comprises 100 points. As the range accuracy of each point on the deck is better than 2 cm in practice, the error in the deck position is small and suitable for guiding the trajectory of the helicopter as it descends to the deck. A plane fitted through these points using least squares then defines the relative distance and orientation of the deck with respect to the helicopter.

We used an *AccuRange 4000* laser rangefinder from Acuity Inc. for this project. This rangefinder uses a modulated beam to measure range using a time-of-flight method. The 20 milliwatt beam is transmitted by a laser diode at a wavelength of 780 nm. The manufacturer claims a stated range of a few centimeters up to 16.5 m with an accuracy of 2.5 mm. Although Acuity provide a line-scanner system of their own, we needed to replace this system to obtain the conical scan pattern peculiar to this application. A mirror was machined out of a block of aluminum with a reflecting face cut at 80° to the axis of the motor. The mirror was hand polished and then electroplated with gold to provide a reflectivity to the laser light of 95%. Figure 2 shows the DASS assembly.

To obtain a fast enough scan rate, we wanted to spin the mirror at a minimum of 1,500 rpm or 25 cycles per second. As the mirror was not symmetrical about the axis, the imbalance of the mirror needed to be addressed to operate at these speeds. We therefore designed a balancing collar out of stainless steel that offset the static and dynamic imbalance of the mirror. The collar was of constant thickness but the end

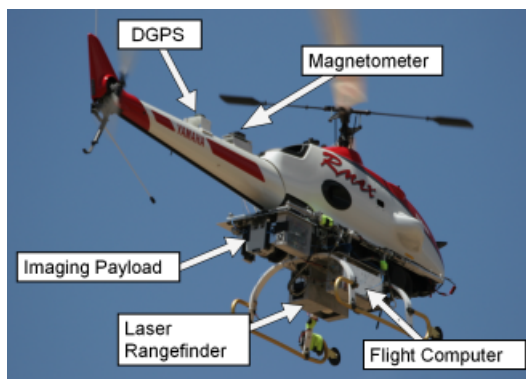


Figure 1: UNSW@ADFA R-Max in Flight during Laser-Range-finding Experiments

profile was machined to maintain the center of gravity of each longitudinal slice of the combined collar/mirror assembly on the axis of the shaft. Once assembled, the balance of the assembly was finely adjusted by adding tiny weights and removing material where required. The entire assembly with LRF and mirror was mounted under the belly of the R-Max using 4 *cable mounts* for vibration isolation. The mounts were tuned to attenuate vibrations at the main rotor frequency and above.

The mirror is mounted directly onto the shaft of a small DC motor, which is itself mounted at 45° to the beam of the LRF. The speed of the motor can be adjusted by changing the input voltage using a multi-position switch. An optical encoder is fitted on the shaft of the motor. The encoder outputs a quadrature pulse train with a precision of 4,096 pulses per revolution. An index pulse is triggered once per revolution for synchronization purposes. The pulse train from the encoder is monitored by an analog safety

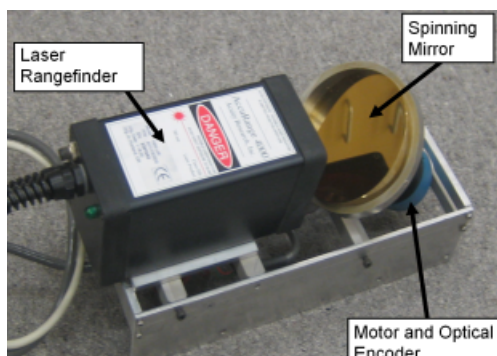


Figure 2: Deck Attitude Sensor Assembly

interlock system that automatically disrupts power to the laser in case of the mirror speed falling below 1,000 rpm. This stops the laser from being concentrated on a single spot for too long and causing a hazard to observers.

The rangefinder and encoder signals are read into a PC104 form factor High Speed InterFace (HSIF) manufactured by Acuity. The HSIF uses an ISA bus interface to communicate with the CPU and enables a sample rate of up to 50,000 samples per second. For our application, to limit the data processing requirements, we have only used a sample rate of 2 kHz but there is no reason why this could not be increased for better accuracy. The HSIF comes standard with a 2 kilobyte hardware buffer. A half-full interrupt on the HSIF triggers a real-time driver program on the PC104 to download the next series of samples and load them into memory. As each sample comprises 8 bytes including amplitude, range, encoder, and intensity fields, the buffer becomes half-full after 128 samples are received. A control thread running on the PC104 executes at 100 Hz and checks for the latest data in RAM each time it is woken up. With a sample rate of 2 kHz, the interrupt is triggered about every 64 ms and takes about 1 ms to execute. The processing takes place after the full data set for each rotation of the mirror is received, which occurs about every 40 ms. Combining all of the latencies together results in a maximum latency of approximately $10+64+1+40 = 124$ ms.

DECK MEASUREMENT ALGORITHM

For each scanned sample, a distance measurement and encoder output are taken from the laser apparatus. The range measurement is corrected for known errors due to changes in temperature, ambient light, and reflectivity. The range measurement is scaled into meters using a lookup table based on calibration data. The encoder measurement is converted to an azimuth angle measured from a reference point designated as the nose of the vehicle. Given an encoder with 4,096 discrete positions per revolution, the azimuth angle (ψ) would be calculated from the encoder output (E) using the

following equation:

$$\psi = 2\pi E/4,096 \text{ (radians)} \tag{1}$$

The range (R) and azimuth angle are then converted into a 3D position relative to the aircraft body axes system, taking into account the mirror geometry. Referring to **Figure 3**, the mirror shaft has a tilt of θ_s and the mirror face is offset from a plane normal to the axis of rotation by angle θ_m .

Assuming that the laser beam departs the rangefinder parallel to the aircraft body x -axis and pointing forward, then the unit vector \hat{u}_m normal to the face of the mirror is given by the following equation:

$$\hat{u}_m = [a \quad b \quad c]^T \tag{2}$$

where

$$\begin{aligned} a &= \cos(\theta_s) \cos(\theta_m) + \sin(\theta_s) \sin(\theta_m) \cos(\psi) \\ b &= -\sin(\theta_m) \sin(\psi) \\ c &= \cos(\psi) \cos(\theta_s) \sin(\theta_m) - \sin(\theta_s) \cos(\theta_m) \end{aligned} \tag{3}$$

From the unit vector \hat{u}_m , the coordinates of each scan point in the aircraft body axes system $[x_b, y_b, z_b]^T$ can be determined by a reflection transformation applied to the incident laser beam striking the mirror. Equation (4) provides the resulting coordinates for each scan point, given the range and the components of the unit vector $[a, b, c]^T$ normal to the mirror. The scan point coordinates are given in aircraft body axes, with the origin being defined as the center of the mirror.

$$\begin{aligned} x_b &= R(1 - 2a^2) \\ y_b &= -2abR \\ z_b &= -2acR \end{aligned} \tag{4}$$

If desired, each 3D point can be adjusted for the attitude (pitch, roll, yaw) of the flight vehicle as measured by the vehicle's attitude reference system. The shift in the position of each point during the scan, due to the velocity of the vehicle, can also be corrected if the velocity is known from another sensor such as GPS. After these transformations, the points are in global

coordinates defined relative to the earth-based axes system $[x_g, y_g, z_g]^T$. Each 3D point is stored into a buffer in the processing unit memory.

After a complete scan, the buffer of 3D points is passed to a subroutine, which calculates the plane of best fit to the stored points. A plane in 3D space is described by equation (5). By determining the coefficients K_1 , K_2 , and K_3 the plane of the surface is then defined.

$$K_1x + K_2y + K_3z = 1 \quad (5)$$

To determine the coefficients describing the plane we use a least-squares method. The objective of the least-squares minimization is to find the value of the plane coefficient vector $\lambda = [K_1 K_2 K_3]^T$ such that the sum of the squares of the error residuals (ε) in equation (6) is minimized.

$$\varepsilon = \sum_{i=1}^n (1 - k_1x_i - k_2y_i - k_3z_i)^2 \quad (6)$$

To implement this, the coordinates of the scan points are arranged in matrix form as per equation (7).

$$A = \begin{bmatrix} x_1 & y_1 & z_1 \\ x_2 & y_2 & z_2 \\ \vdots & \vdots & \vdots \\ x_n & y_n & z_n \end{bmatrix} \quad (7)$$

Equation (8) represents a solution to the least square problem.

$$\lambda = (A^T A)^{-1} A^T b \quad (8)$$

where

$$b = [1 \quad 1 \quad \dots \quad 1]^T$$

Once the equation of the plane is found from equation (8), the instantaneous height H of the vehicle above the surface can be found using the following equation:

$$H = -\frac{1}{K_3} \quad (9)$$

Likewise, the roll and pitch of the surface can be found from the equation of the plane. If we de-

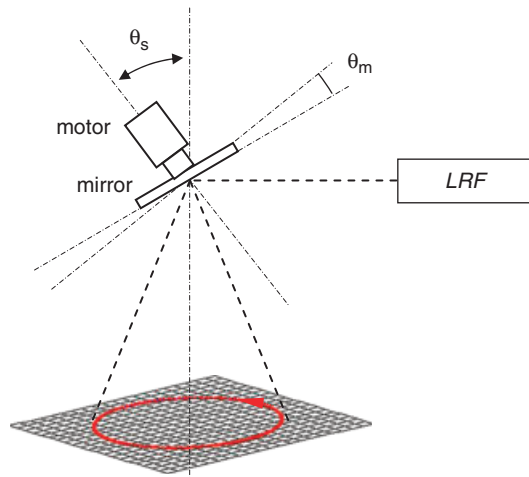


Figure 3: Mirror Geometry

fine pitch angle θ as the inclination of the plane from the y -axis and roll ϕ as the inclination of the plane from the x -axis, then equation (10) defines the orientation of the plane.

$$\theta = \arcsin(K_1) \quad \phi = \arctan\left(\frac{K_2}{K_3}\right) \quad (10)$$

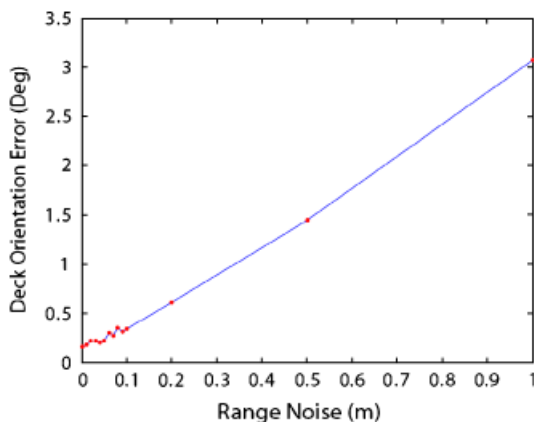
When the helicopter is flying at a high altitude, the oval scan pattern drawn on the deck below will be quite large and for a small deck this can cause the oval to partially fall off the edge of the deck. Large helicopter pitch and roll changes can also translate the oval so that part of the oval is no longer on the deck. To deal with this, we have two strategies. Firstly, in the production version, we intend to adjust the mounting bracket design so that the laser is tilted forward during hover such that the rear arc of the scan pattern lies more or less underneath the center of gravity of the helicopter. This way, regardless of altitude, there will always be part of the oval that lies on the deck, provided the helicopter is overhead. Parts of the oval that are not within a predefined radius of a point directly below the helicopter will be disregarded. Secondly, we have refined the deck estimation algorithm to disregard points that are not within some tolerance of the current deck estimate. The aim of this is to eliminate parts of the scan pattern, which are not on the deck by neglecting those points, which are not close to the plane of where we believe the deck to be. This is achieved using a simple

iterative process. First, the distance between every scanned point and the estimated plane of the deck is calculated. Any points that are outside of a certain tolerance are ignored. If the percentage of points being ignored becomes too high or too low, the tolerance is adjusted. A new deck estimate is then calculated and stored. A further strategy can be used in conjunction with the visual sensor. As the vision sensor provides a measure of the helicopter's lateral and longitudinal position with respect to the center of the deck, it can be used to eliminate parts of the scan pattern that are known *a priori* to lie outside of the known boundaries of the landing platform.

SENSOR SIMULATION RESULTS

We have developed a Simulink representation of the LRF sensor including the deck estimation algorithm. The deck position calculation algorithm was run with various amounts of white noise added to the range data to test the tolerance of the algorithm to noise. The set of error results presented in **Figure 4** are from simulations of the scanning algorithm at a 10 m height above a flat moving platform. The platform was simulated to move at a sinusoidal rate in both roll and pitch. As can be seen from the results, there is an almost linear relationship between the roll and pitch calculation error and the amount of simulated range noise. Importantly, the algorithm is seen to be very resilient to noise, demonstrated by a $<0.5^\circ$ error with up to 10 cm of noise in the laser range finder. Increasing the range noise to an unrealistic level of 50 cm only

Figure 4: Effect of Noise on Deck Attitude Sensing System (DASS) Accuracy



increases the roll and pitch calculation error to within 1.5° .

FLIGHT TEST OF LASER SENSOR

Our flight test experiments consisted of three parts: determination of attitude, determination of height, and closed-loop control of height. In the first part, we wanted to determine how well the laser sensor worked at measuring orientation. As we did not have access to a moving deck platform at the time, we chose instead to have a stationary ground plane and stimulate the attitude of the helicopter through the pilot controls. We did not transform the coordinates of the scanned points into earth-centered coordinates, so that the attitude of the measured deck plane would correspond to the attitude of the helicopter.

By comparing the attitude measured by the Yamaha Attitude Sensor (YAS) with the deck orientation estimated by the laser system, we were able to check whether the system was working. The R-Max was flown over a grass runway and made to roll and pitch while in hover. The comparison of the laser output and the YAS is shown in **Figure 5**.

There is a clear correlation between the two sensing systems, with some minor deviations. The height output of the algorithm also compares well with the altitude output of the NovAtel DGPS system after subtracting the elevation of the ground under the helicopter from the DGPS altitude. The results of this comparison, in **Figure 5c**, show a very close match between the two systems.

The final tests involved using the laser system to control the height of the helicopter. A simple PID controller was used to control the collective pitch of the main rotor to maintain a constant altitude. The controller gains were tuned manually starting from a low value. On handover to the helicopter flight computer, the desired altitude fed to the control system was set to the current altitude measured by the laser system. The control system was able to keep the

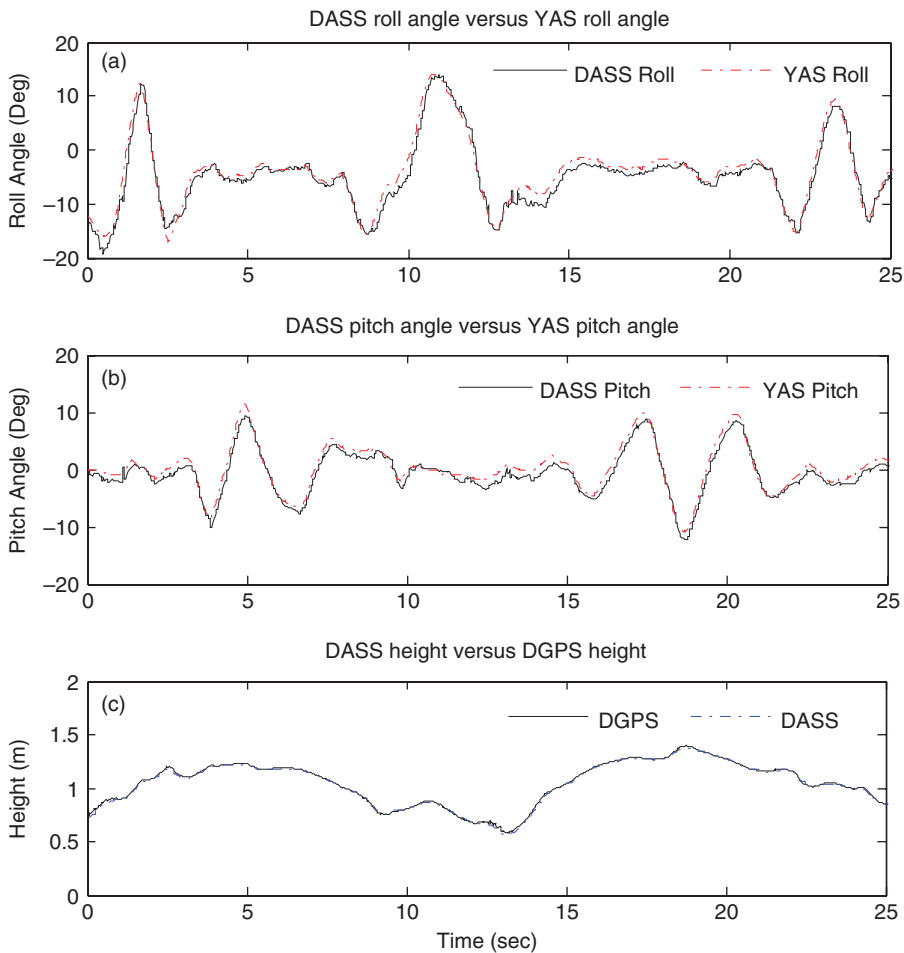


Figure 5: Laser Rangefinder (LRF) Flight Test Data

helicopter to within 10 cm of the desired altitude despite strong wind gusts on the day.

The same controller was then extended to control of landing. In this case, with the control handed over to the PID controller, a command sent from the ground control station initiated a gradual change in the reference height to be made. The flight control software decreased the desired height by 3 cm/s. In response, the helicopter descended from its initial hover height until it came in contact with the ground. For future work, this descent speed will be increased several fold as it is very conservative.

Visual Tracking Sensor

The concept of using vision to land a UAV on a moving deck is not new. Montgomery et al. (2003), at the University of Southern California,

have landed a small autonomous helicopter on a helipad using vision and inertial information. In their work, a pattern comprised of polygons painted on the helipad was identified and tracked using a fixed threshold to pick out the pattern from the background. The helicopter was able to track the pattern even when the helipad was moving; however, the helipad motion was switched off for the actual landing.

In previous work, one of the authors (Garratt and Chahl 2003) has used a system of three visual landmarks on the ground to control a small 7 kg helicopter in hover. Such systems could all be used in theory to hover over the deck of the ship; however, all of these systems suffer from the problem of losing track. For the problem of a moving ship's deck, there is concern that, at times, sea spray could obscure parts of a pattern

or that with the combined motion of the ship and helicopter, parts of the pattern could disappear from the field of view at times.

For best accuracy, the aim is to have as much of the field of view as possible taken up by the pattern. However, a larger pattern in the field of view results in a greater likelihood of part of the pattern being lost due to relative motion effects. For this reason, we propose using a single light source, or *beacon*, as the target that would be centered in the field of view where practicable. Such a target would be the least likely to disappear from view and the use of a single bright point light source target simplifies the tracking problem significantly. In conjunction with our laser sensor, a single beacon is all that is required to fix the position of the helicopter with respect to the center of the deck. While the yaw angle of the helicopter is not determined using the combination of a point target and laser scanner, we have found the yaw loop very easy to control using a simple PD feedback scheme based on heading angle, and all that is required is a system to tell the helicopter what heading to steer to match the course of the ship. This would only require a slow update as ships take a long time to change course when underway.

A single light source, or beacon, is used as the target, which is centered in the field of view where practicable. In conjunction with the laser sensor, a single beacon is all that is required to fix the position of the helicopter with respect to

the center of the deck. We have used a bright LED for the beacon. We have settled on a peak wavelength of 650 nm, which is better than the near infra-red wavelengths that would suffer more, given the waterborne application. **Figure 6** shows the R-Max hovering above the beacon used for our experiments.

Rejection of unwanted specula reflections and other lights is possible by choosing a narrow-band filter matched to the spectral output of the beacon, which in turn is ideally chosen where atmospheric absorption is minimized. An alternative proposal is to make use of a color camera or image sensor, so that if a narrowband red beacon was being used, for example, other bright pixels that are not the target and that have a significant blue or green intensity relative to the red intensity can be discounted.

Our current image sensor is achieved through the use of a monochrome CMOS image sensor, with all of the necessary image processing and coordinate determination located within a single FPGA. The FPGA algorithm interfaces to the flight control system and delivers the coordinates of the beacon within the image field to the flight computer.

The optics used to image onto the sensor defines the positioning accuracy and the initial capture range of the beacon. We have used a lens with 6 mm focal length and red narrowband optical filters to improve rejection over the specula reflections expected in the water environment. Other lenses can be easily mounted to achieve a desired FOV (field of view). The beam pattern may be narrowed, increasing the output aperture, in which case more of the sensor will be illuminated by the beacon.

The pixel intensity data are delivered to the adjacent FPGA, upon which the first of two pipelined algorithms are run. This algorithm monitors the live pixel stream to locate adjacent pixels of brightness above a certain threshold, and determines whether to consider these as contenders for the beacon. As the determination

Figure 6: Hover of R-Max Over Beacon



of the area of the region must be taken as pixels are rastered from the sensor, the leftmost column and run length within that row are remembered for each of a finite number of regions, as is the first encountered row. As rows are analyzed the boundaries of each region are moved outwards to the farthest contiguous breadth and height, hence the left, top, right, and bottom encompass each region contender in the frame. From this the rectangular area is obtained, and the horizontal and vertical centers are easily determined. The intensity threshold is updated at the end of each frame based on a fixed percentage of the peak pixel value within that frame that is remembered during the streaming, and is applied during the following frame on the assumption that there will be little inter-frame change.

The computed centers of the regions are analyzed, with the centers and areas stored. With an appropriately tuned spatial and temporal filter, areas that are not the target (such as specular reflections from the sea surface) can be rejected while tolerating smaller motions due to atmospheric-induced scintillation effects and motion caused in the image field by vehicle and landing platform alike. The most likely location for the beacon based on area and intensity is chosen for each frame. A very compact 8052-like micro-processor (implemented within the FPGA) is

used to compute an azimuth and elevation angle measured from the tracking sensor to the beacon, based on the pixel location delivered by the tracking algorithm. This calculation takes into account the focal length of the lens in use, so that it could be adjusted in real time if a motorized lens was used. These angles are then forwarded to the flight computer. Should no reliable beacon be determined from this stage, no coordinate is sent in that frame time.

During processing, the image sensor must be controlled in exposure and frame rate in order to optimize the imaging of the beacon. This is done within the FPGA, by a simple algorithm that analyzes the size of the beacon (in pixels) and controls the image sensor to always contain this size within a certain range. The exposure can be adjusted in steps of 25.4 μ s for the fastest possible pixel clock, up to the full frame rate.

Our beacon tracking system has been designed to be lightweight, self-contained, and to have low power consumption. The latter is achieved through the use of a mega-pixel CMOS image sensor that uses only 363 mW, and locating all of the necessary image processing and coordinate determination within a single *Xilinx Spartan IIE* FPGA. The image sensor used is a monochrome mega-pixel 1/2" format, Micron MT9M001,

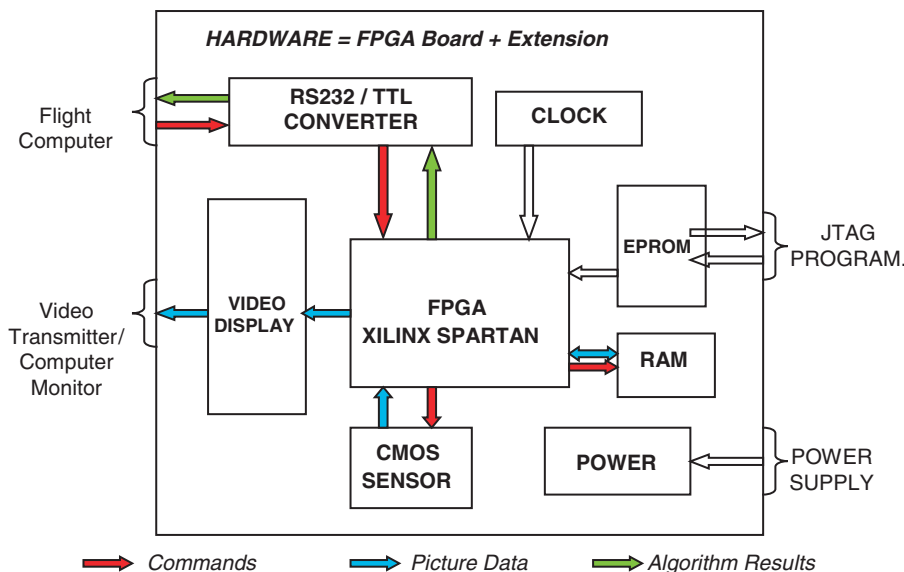
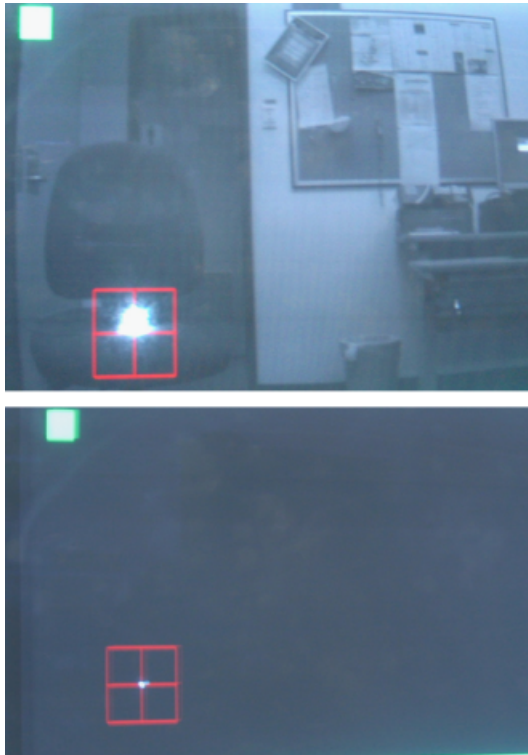


Figure 7: Tracking Sensor Hardware

Figure 8: Typical Diagnostic Image from the Beacon Tracking Is Achieved on a Computer Monitor with a Graphical Overlay, All Generated from the Field Programmable Gate Array (FPGA). The two images shown here are for an overexposed image with no filter (top) and a correctly exposed image (bottom).



with $5.2 \mu\text{m}^2$ 10 bit pixels and a published sensitivity of $2.1\text{V}/\text{lux s}$. **Figure 7** shows the architecture of our tracking sensor.

The FPGA interfaces to the flight control system using RS232, and provides extra diagnostics in the form of XGA (eXtended Graphics Array format comprising 1024×768 pixels) imagery to

Figure 9: UNSW @ADFA R-Max Hovering over a Moving Deck Simulator.



an external monitor. Using an onboard video converter, we are able to see the image using a 2.4 GHz composite video downlink to the ground. The Philips I2C bus is used to configure the sensor on the fly, based on optimizations computed adaptively in the FPGA. The FPGA delivers the coordinates of the beacon within the image field to the flight computer using RS232. For diagnostics, a red cross hair is superimposed on the video output at the chosen center, and a green square overlay indicates a locked beacon. An indication of this imagery is shown in

Figure 8.

Tests in a variety of light levels within the laboratory have been undertaken with visually apparent robustness, even in the presence of strobing between fluorescent lights and the frame rate. We have been able to track the beacon from 100 m away in bright sunlight.

Moving Deck Simulator

We have constructed a moving deck simulator (**Figure 9**) to test the landing sensors and the ability of our deck-lock system to restrain the helicopter upon landing. The landing deck is a square of dimensions $3 \text{m} \times 3 \text{m}$ and consists of an aluminum frame upon which a stainless-steel wire mesh is supported. Spring-loaded probes on the feet of the helicopter undercarriage engage with the square mesh to prevent the helicopter from sliding once it has touched down.

Using three actuators, the deck allows for three degrees of freedom of motion: pitch, roll, and heave. The deck is capable of 1 m of heave and up to 25° of pitch and roll motion with a period as low as 7 s. Our in-house software currently allows us to represent ship motion as sinusoidal, where the phase and amplitude of each degree of freedom can be controlled separately. Eventually, we aim to drive the deck to match real ship motion data.

To reduce cost and complexity, we have limited the design of the moving deck simulator to produce the key ship motions of heave, pitch, and

roll rather than generate all six degrees of freedom. This has been achieved by a central column fixed to the center of the deck. A universal joint between the deck and the central column allows the deck to pitch and roll but prevents yaw. The central column is able to move vertically but is prevented from sideways motion using rollers along its length. The actuators are arranged vertically with their bases on the corners of an equilateral triangle of side length 1.5 m. Ball joints on the top of the actuators connect them to the underside of the deck.

By varying the length of each actuator, any combination of pitch, roll, and heave can be achieved. The *Thompson TC5* linear actuators use electrically driven ball-screws to deliver up to 3,000 N and 1 m/s of motion. A system of counterbalances is used to offset the weight of the deck and fixtures, and so the load on the actuators is limited to that required to overcome inertia and friction. The actuators are driven by *Copley Xenus* controller amplifiers, which are connected to a field-hardened personal computer (PC) using a CAN bus network. The computer calculates the desired trajectory of each actuator to achieve any arbitrary pitch, roll, and heave motions and updates the trajectories using the CAN bus connection.

Conclusion

We have described systems for enabling a rotary wing UAV to launch and land on a moving ship's deck at sea. These systems are smaller and less costly to produce than existing systems and will allow much smaller UAVs and ships to be integrated with each other. In future work, we will use the combined image sensor and DASS to perform an autonomous landing onto the moving deck platform.

Acknowledgment

This work has been supported by an Australian Research Council Linkage project grant in conjunction with industry funding from UAV Australia Pty Ltd.

References

- Belton, D., S. Butcher, G. Ffoulkes-Jones, and J. Blanda, "Helicopter recovery to a moving platform using a GPS relative positioning system." Proceedings of the 12th International Technical Meeting of the Satellite Division of the Institute of Navigation, pp. 1769–1776, Nashville, TN, September 14–17, 1999.
- Charles, J., "CMU's autonomous helicopter explores new territory," *Intelligent Systems and Their Applications*, Vol. 13, No. 5, pp. 85–87, 1998.
- Doherty, P., "Advanced research with autonomous unmanned aerial vehicles." Proceedings of the 9th International Conference on Knowledge Representation and Reasoning, 2004.
- Ford, T., M. Hardesty, and M. Bobye, "Helicopter ship board landing system." Proceedings of the 18th International Technical Meeting of the Satellite Division of the Institute of Navigation, Long Beach, CA, 2005.
- Garratt, M.A. and J.S. Chahl, "Visual control of a rotary wing UAV." UAV Asia-Pacific Conference. Flight International, February 2003.
- Gold, K. and A. Brown, "An array of digital antenna elements for mitigation of multipath for carrier landings." Proceedings of ION 2005 National Technical Meeting, pp. 26–28, San Diego, CA, January 2005.
- Gold, K.L. and A.K. Brown, "A hybrid integrity solution for precision landing and guidance." Position Location and Navigation Symposium, pp. 165–174. IEEE, April 26–29, 2004.
- Johnson, E.N. and D.P. Schrage, "The Georgia Tech unmanned aerial research vehicle: GTMax." Proceedings of the AIAA Guidance, Navigation, and Control Conference, Austin, TX, August 11–14, 2003.
- Kim, H.J., D.H. Shim, and S. Sastry, "Flying robots: Modeling, control, and decision-making." International Conference on Robotics and Automation, May 2002.
- Montgomery, J.F., S. Saripalli, and G.S. Sukhatme, "Visually guided landing of an unmanned aerial vehicle," *IEEE Transactions on Robotics and Automation*, Vol. 19, No. 3, pp. 371–380, 2003.
- Montgomery, P.Y., D.G. Lawrence, K.R. Zimmerman, H.S. Cobb, G.M. Gutt, C.E. Cohen, and B.W. Parkinson, "UAV application of IBL for autonomous takeoff and landing." Proceeding of the 12th International Technical Meeting of the Satellite Division of the Institute of Navigation, pp. 1541–1547, 1999.

NovAtel Inc., "Relative moving baseline software," Technical report, March 2000. Available at (http://www.novatel.com/products/waypoint_techreports.htm) accessed March 28, 2008.

Pervan, B., F. Chan, D. Gebre-Egziabher, S. Pullen, P. Enge, and G. Colby, "Performance analysis of carrier-phase DGPS navigation for shipboard landing of aircraft," *Journal of the Institute of Navigation*, Vol. 50, No. 3, pp. 181–191, 2003.

Sierra Nevada Corporation, "UCARS-V2 UAS common automatic recovery system – version 2." Available at (<http://www.sncorp.com/prod/atc/uav/default.shtml>) accessed March 28, 2008.

US Air Force, "Joint precision approach and landing system (JPALS) operational requirements document." USAF 002-94-1, 1994.

Whalley, M., M. Freed, M. Takahashi, D. Christian, A. Patterson-Hine, G. Shulein, and R. Harris, "The NASA/Army autonomous rotorcraft project." Proceedings of the American Helicopter Society 59th Annual Forum, 2003.

Author Biographies

Matt Garratt is the principle author and is a lecturer at The University of New South Wales at the Australian Defence Force Academy (UNSW@ADFA). Before becoming a lecturer in 2001, he served for 10 years in the Royal Australian Navy, working as a dual specialist in alternate aeronautical and marine engineering postings. Matt completed his Ph.D. at the Australian National University in 2008. His main

research areas are helicopter dynamics and sensing and control for autonomous systems.

Himanshu Pota received his Ph.D. from the University of Newcastle, Australia, in 1985. He is currently an Associate Professor with UNSW@ADFA. He has a continuing interest in the area of power system dynamics control and modeling control of mechanical systems such as flexible structures, acoustical systems, and UAVs.

Andrew Lambert lectures in Electrical Engineering at UNSW@ADFA. He obtained his B.S. (Hons) in Physics from University of Otago, New Zealand, in 1987, and his Ph.D. on Optical Image Processing from UNSW in Electrical Engineering in 1997. He specializes in signal and image processing, optoelectronics, and high-speed DSP and FPGA hardware.

Sebastien Eckersley-Maslin received his B.E. (Electrical) from UNSW@ADFA in 2003. He is currently completing a Masters in electrical engineering while serving as a Weapons Electrical Engineering Officer in the Royal Australian Navy.

Clement Farabet is currently completing his M.Eng. in Electrical Engineering from the National Institute of Applied Sciences, France. He worked for a year at UNSW@ADFA with Dr. Matt Garratt, on several projects involving UAVs. He is now doing his Final Year's Thesis at New York University.